

Significant local sea level variations caused by continental hydrology signals

Rebecca McGirr¹, Paul Tregoning², Anthony Patrick Purcell², and Herbert W. S. McQueen²

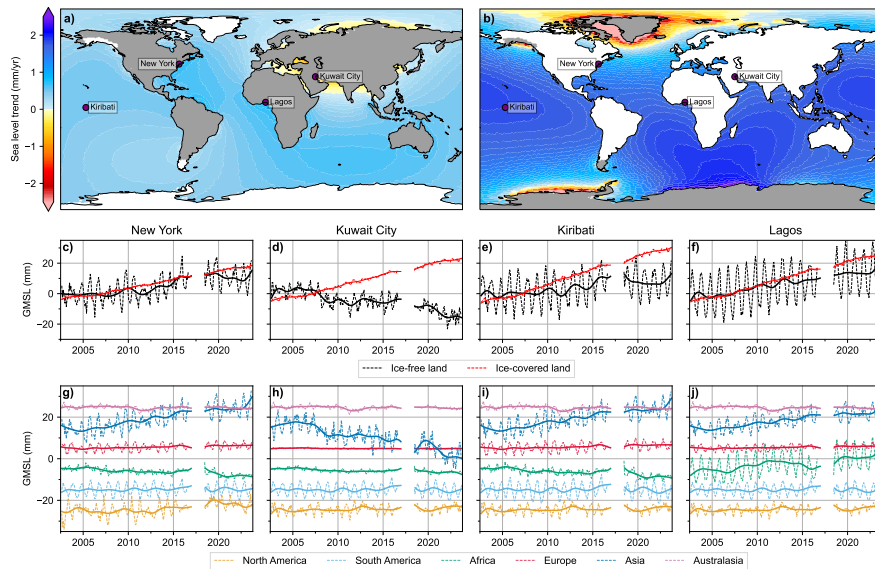
¹ANU

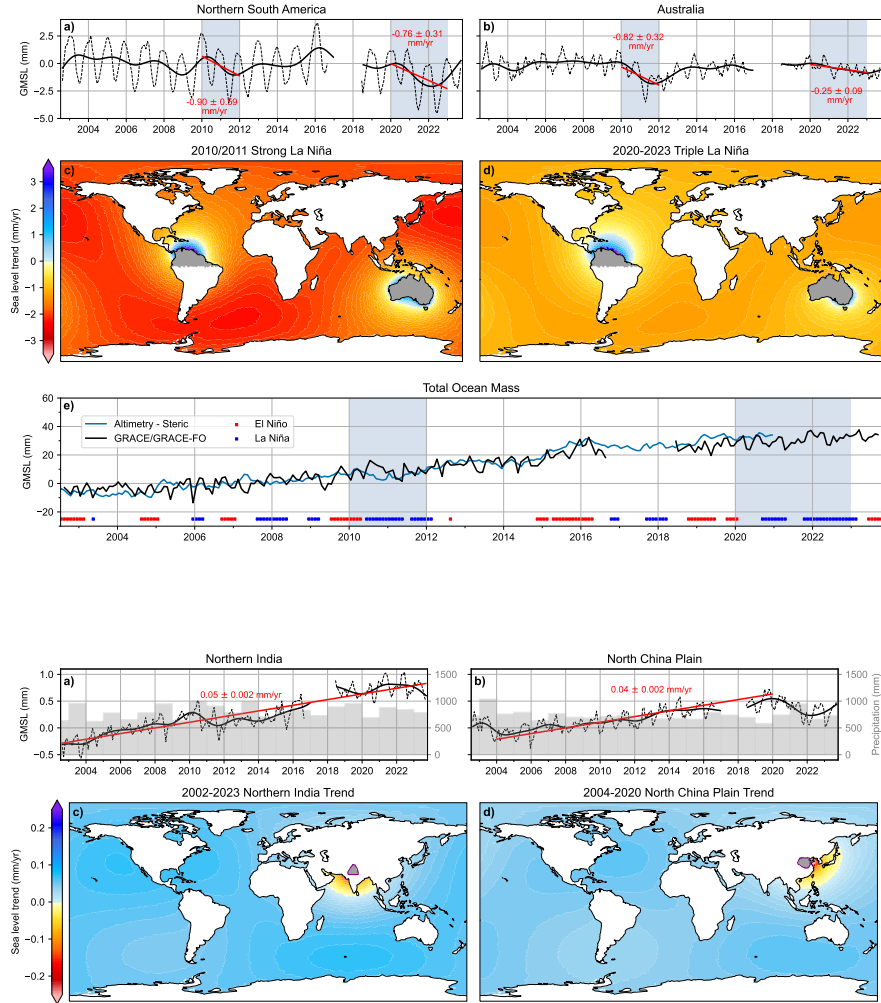
²Australian National University

March 07, 2024

Abstract

Space gravity missions have enabled the quantification of ocean mass increase over the past two decades due to exchanges between continents and oceans. Globally, non-steric sea level rise is predominantly driven by melting polar ice sheets and mountain glaciers. However, continental hydrological processes also contribute to sea level change at significant magnitudes. We show that for most coastal areas in low-to-mid latitudes, up to half of local non-steric sea level rise is due to changes in water storage in ice-free continental regions. At other locations the direct attraction effect of anthropogenic pumping of groundwater over the duration of the GRACE and GRACE-FO mission offsets sea level rise from ice sheet and glacier melt. If these trends in continental hydrological storage were to slow or stop, these regions would experience greatly accelerated sea-level rise, posing a risk to coastal settlements and infrastructure, however, sea level rise elsewhere would be reduced.





1 **Significant local sea level variations caused by**
2 **continental hydrology signals**

3 **Rebecca McGirr^{1,2}, Paul Tregoning^{1,2}, Anthony Purcell¹, Herb McQueen¹**

4 ¹Research School of Earth Sciences, Australian National University, Canberra, ACT, 0200, Australia

5 ²The Australian Centre for Excellence in Antarctic Science, University of Tasmania, Hobart, Tasmania
6 7001, Australia

7 **Key Points:**

- 8 • Exchange of water between continents and oceans causes global sea level change
9 at rates comparable to the contributions of ice sheets
10 • The direct gravitational attraction effect on local sea level is of a larger magni-
11 tude than the far-field sea level changes
12 • Inter-annual continental hydrology signal impacts on local sea level have negated
13 the impacts of melting polar ice sheets in some locations

Abstract

Space gravity missions have enabled the quantification of ocean mass increase over the past two decades due to exchanges between continents and oceans. Globally, non-steric sea level rise is predominantly driven by melting polar ice sheets and mountain glaciers. However, continental hydrological processes also contribute to sea level change at significant magnitudes. We show that for most coastal areas in low-to-mid latitudes, up to half of local non-steric sea level rise is due to changes in water storage in ice-free continental regions. At other locations the direct attraction effect of anthropogenic pumping of groundwater over the duration of the GRACE and GRACE-FO mission offsets sea level rise from ice sheet and glacier melt. If these trends in continental hydrological storage were to slow or stop, these regions would experience greatly accelerated sea-level rise, posing a risk to coastal settlements and infrastructure, however, sea level rise elsewhere would be reduced.

Plain Language Summary

It is well understood that melting of polar ice sheets and mountain glaciers cause increases in ocean mass, leading to a corresponding rise in global sea level. What is not as obvious is that multi-year changes in the storage of water on continents not covered by ice also contribute significantly to changes in global sea level. Over recent years and in some locations, the magnitude of these ‘continental hydrology’ contributions to sea level changes have been comparable to the contributions of the ice-covered regions. In some cases, the former have offset the ice sheet contributions, thus reducing regional sea level rise to substantially smaller magnitudes. Through an analysis of space gravity data, we have quantified the effects of continental hydrology on regional sea level and show that changes caused both naturally (e.g. through La Niña events) and through anthropogenic activities (e.g. extraction of groundwater) can increase or decrease regional sea level by significant amounts.

1 Introduction

Increases in ocean mass has risen global mean sea level at a rate of 2.5 ± 0.4 mm/yr (Tapley et al., 2019); however, the most important impact of sea level variations on society lies in the local changes rather than global averages. Ocean mass variations are predominantly caused by movement of water, including mass balance change of polar ice sheets (Velicogna & Wahr, 2013; Tapley et al., 2019) (Greenland and Antarctica) and glaciated regions (Wouters et al., 2019; Ciraci et al., 2019) (e.g. Alaska, Patagonia, Svalbard), and changes in soil moisture, surface water and groundwater on continents (Leblanc et al., 2009; Rodell et al., 2019). Closure of the sea level budget has been the focus of many studies (e.g. Barnoud et al., 2023) and involves the apportioning of contributions from polar ice sheets, mountain glaciers, and terrestrial water storage which are further amplified by steric expansion of the oceans as they warm. Rather than considering local sea level changes, studies of this process tend to focus on integrated sea level signals over the global oceans and use a combination of ocean height changes measured by satellite altimetry, ocean mass change from space gravity missions and temperature and salinity changes in the oceans from Argo floats (Roemmich et al., 2009) and expendable BathyThermograph observations (e.g. Boyer et al. (2016)).

Exchanges of water between continents and oceans includes three additional components that directly affect ocean height beyond the simple volumetric effect. First, variations in the water mass on the continent change the direct gravitational attraction between the oceans and continents (Mitrovica et al., 2001; Lambeck et al., 2017). This process can have a significant effect on local sea level near the location of change of continental water source (J. Sun et al., 2022). Second, water added or taken from the oceans moves the centre of mass of the Earth and is redistributed on a rotating Earth accord-

ing to particular spatial patterns (Mitrovica et al., 2001; Tamisiea et al., 2010) and affects sea level in the far-field. Third, elastic deformation of the ocean floor occurs due to changing ocean mass loads (Mitrovica et al., 2001, 2011), affecting both near-field and far-field ocean heights. Sea level fingerprints (Tamisiea et al., 2010; Kim et al., 2019; J. Sun et al., 2022) can be used to calculate the spatial pattern of change of ocean height related to mass changes on land.

The Gravity Recovery and Climate Experiment (GRACE) and GRACE Follow-On (GRACE-FO) space gravity missions provide near-continuous data from 2002 to present from which estimates of change in mass distribution on Earth can be made (Tapley et al., 2004, 2019). The leakage of signals between continents and oceans has been problematic in the analysis of space gravity data when estimating changes in mass distribution using spherical harmonic basis functions (Chen et al., 2009; Velicogna & Wahr, 2006). Various re-scaling strategies have been invoked (Watkins et al., 2015; Wiese et al., 2016), as well as novel forward modelling approaches to re-instate leaked signal back to the likely correct location on the continents (Chen et al., 2009; Jeon et al., 2021). The use of mass concentration elements (mascons) (Mueller & Sjogren, 1968), rather than spherical harmonics, helps to reduce the leakage of signal by permitting more direct spatial constraints on parameters to be applied (Rowlands et al., 2005; Watkins et al., 2015; Tregoning et al., 2022). Irregular-shaped mascons, that follow coastlines with an accuracy of <9 km, further reduce the leakage of signal between continents and oceans (Tregoning et al., 2022).

Through the use of forward modelling of GRACE estimates of terrestrial water storage change and sea level fingerprints, agreement was found between regional ocean height changes and those observed by satellite altimetry (Jeon et al., 2021). A similar forward-modelling approach was used to estimate a 0.32 mm/yr terrestrial water storage contribution to global sea level, leading to a tighter closure of the total sea level budget (Kim et al., 2019). Contributions to global sea level by each continent (plus Greenland and Antarctica) have been assessed in the literature (Rodell et al., 2019).

Separating the contributions from ice-covered regions and the rest of the continental land areas permits a more detailed assessment of how continental hydrological processes affect the spatial pattern of sea level height change. The latter includes ground-water variations, impounding of water in dams and reservoirs, and changes in soil moisture volumes. We quantify the integrated change of these components, or total water storage (TWS), from an analysis of GRACE/GRACE-FO measurements. We then convolve these mass changes with sea level fingerprints to construct time series of regional ocean mass change, caused by continental hydrology (i.e. excluding ice-based mass changes) to identify the continental hydrology sources of changes in local sea level at certain locations.

2 Space gravity data analysis

We estimate changes in mass on Earth as a change in height of a water column on 12,755 irregularly shaped mascons using the range acceleration as the key inter-satellite observation of the GRACE and GRACE Follow-On space gravity missions (Allgeyer et al., 2022). Data from August 2002 to September 2023 were processed, using the hybrid ACH1B data to model the non-gravitational accelerations on the GRACE-D satellite (Harvey et al., 2022). Non-linear effects in accelerometer measurements, caused by thermal variations within the satellites, were mitigated using a high-pass filtering approach (McGirr et al., 2022). This enables the number of accelerometer calibration parameters to be limited to one bias and one scale per day per orthogonal axis for the GRACE data and for GRACE-FO data up to the end of 2022. We computed degree-1 contributions from a combination of GRACE and ocean model data (Y. Sun et al., 2016) and the $C_{2,0}$ estimates were replaced with values derived from satellite ranging data (Loomis et al., 2020). The values of $C_{3,0}$ were also replaced for the GRACE-FO data. We formed normal equa-

115 tions for 24-hour orbital arcs, then stacked these daily normal equations to form monthly
116 solutions, defined using calendar months.

117 We regularise the solutions to overcome the noise inherent in inversions of space
118 gravity data, applying the same values to mascons using broad spatial regions. The off-
119 diagonal elements of our regularisation matrix are zero and the diagonal elements are
120 $1/\sigma^2$ as shown in Figure S1. The regularisation matrix is applied for each day included
121 in the monthly solution and we use the same regularisation for each monthly solution
122 to keep the analysis process as generic as possible.

123 **3 Calculation of sea level fingerprints**

124 For a 1 m change in water storage on each land mascon, we calculated the corre-
125 sponding change in water height of each ocean mascon (the code used for this calcula-
126 tion is that employed by Lambeck et al. (2017)). We include in the computations the
127 rotational, gravitational and elastic deformation signals caused by the mass exchange be-
128 tween land and oceans. The computations are done on a radially symmetric, spheroidal
129 elastic Earth using the elastic structure of the PREM model (Dziewonski & Anderson,
130 1981). Visco-elastic effects are insignificant and have not been included because the mag-
131 nitudes of load variations are small (<15 m) and the time scale of the variations is short
132 (<1 month). The monthly mass changes on land are multiplied by the computed finger-
133 prints to apportion the signals over the oceans, thus deriving corresponding monthly ocean
134 signals.

135 **4 Results**

136 **4.1 Terrestrial water storage contributions to sea level**

137 We are interested in the ocean mass changes from continental hydrology signals.
138 To isolate these signals from ice-related signals over continents, we excluded mass changes
139 over Greenland, Antarctica, the Alaskan and Patagonian glaciers as well as the ice-covered
140 regions of Northeast Canada (Baffin Island, Ellesmere Island), Svalbard and Russian Arc-
141 tic islands (Severnaya Zemlya and Novaya Zemlya). We calculated separately the ocean
142 mass changes caused by these excluded regions.

143 Continental hydrology signals in ice-free regions (grey areas; Figure 1a) contribute
144 23% to the global ocean mass budget, with the remaining portion (77%) accounted for
145 by melting mountain glaciers and ice-sheets which are predominantly found at high lat-
146 itudes (grey areas; Figure 1b). Although the contribution of ice-covered regions to global
147 mean sea level is ~ 3 -times greater than ice-free regions, these continental hydrology sig-
148 nals contribute significantly to regional rates of sea level change. The rate of ocean mass
149 increase from continental hydrology over the GRACE and GRACE-FO era has a distinct
150 spatial pattern driven predominantly by total water storage (TWS) trends in Asia (Fig-
151 ure 1a). Meanwhile, the spatial pattern of the sea level fingerprint due to ice-melt causes
152 near-uniform sea-level rise in mid-to-low latitude areas (Figure 1b). The fingerprint of
153 continental hydrology contributions to sea-level results in both the mitigation or ampli-
154 fication of ocean mass increase due to melting ice at different locations (Figure S2).

155 Declining TWS in Asia over the GRACE and GRACE-FO era has led to an increase
156 of up to 0.8 mm/yr around Africa, across the central Atlantic Ocean, around Australia
157 and surrounding Pacific Island nations and in the North Pacific Ocean. The significant
158 reductions in continental hydrology contributions of ocean mass in the Black Sea, east-
159 ern Mediterranean Sea and the Persian Gulf are caused by decreased strength in the di-
160 rect gravitational attraction due to declining TWS in Asia since 2002, including around
161 -0.1 mm/yr due to decreased water storage in the Caspian Sea. Although typically less
162 than 1 mm/yr, local ocean mass changes driven by continental hydrology are compara-

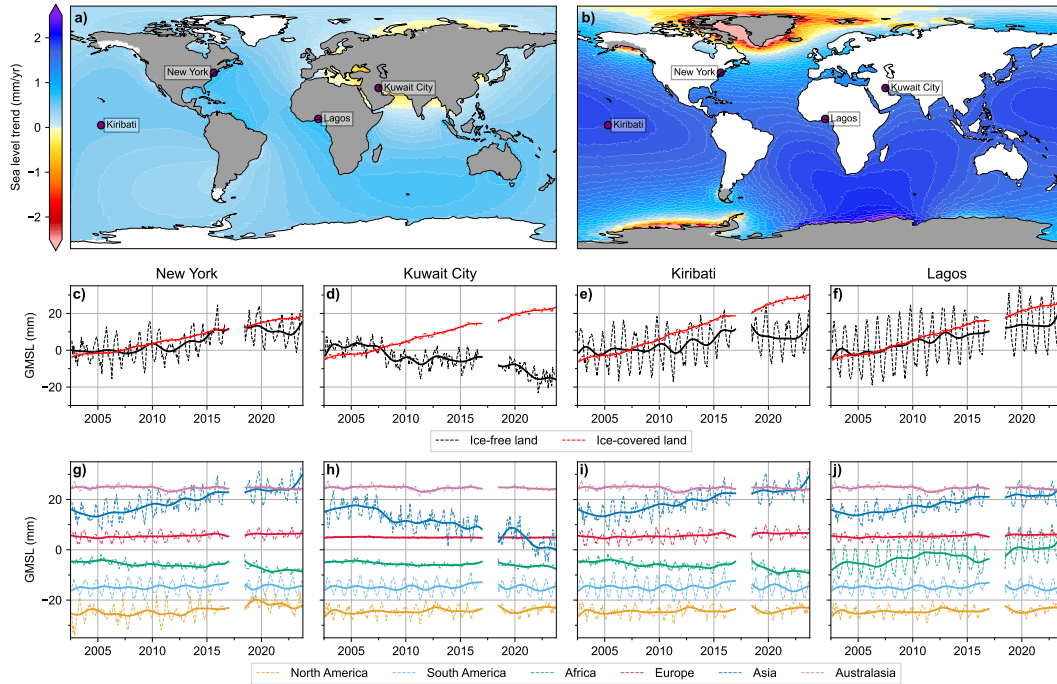


Figure 1. Rate of ocean mass change due to (a) continental hydrological processes, excluding ice-related signals (b) ice-covered regions. Mascons used to compute the ocean signals from continental hydrology in specific regions are indicated (grey). (c-f) time series of global mean sea level (GMSL) changes at sites indicated in a) from ice- and continental-related ocean contributions. Monthly values (dashed lines) and low-pass filtered values (solid) are plotted. (g-j) Contributions of six continental regions (as defined in Figure S3) to the changes in ocean mass at each location (each time series is offset by 10 mm).

163 ble to or greater than individual contributions of the Greenland (+0.77 mm/yr) and Antar-
 164 tic (+0.33 mm/yr) ice sheets over the past two decades (Rodell et al., 2019; Tapley et
 165 al., 2019).

166 **4.2 Local sea level changes**

167 The spatial variability of the contributions of both ice-based and continent hydro-
 168 logy to ocean mass change creates a complex pattern from which to extract a compre-
 169 hensive synthesis of local information. We focus on particular locations where the mag-
 170 nitudes of rates of continental hydrology contributions are high.

171 The largest increase in ocean mass caused by continental hydrology occurs around
 172 the coast of the Gulf of Guinea, central-west Africa near Lagos (Figure 1a). The increase
 173 in total ocean mass during the GRACE period near Lagos amounts to ~ 18 mm of which
 174 36% is derived from contributions from continental hydrology (Figure 1f). Similarly, along
 175 the east coast of North America, the magnitude of ice- and continent-based contribu-
 176 tions is comparable from 2002-2019, at ~ 13 mm, as seen in the time series for New York
 177 (Figure 1c). Interestingly, the decline at New York of sea level change contributions from
 178 continental hydrology after 2020 occurs because of the reduced contributions from Asia
 179 and increased wetting of the African continent drawing more water from the oceans (Fig-
 180 ure 1g).

181 In contrast, the total ocean mass change at Kuwait City in the western Persian Gulf
 182 is only ~ 12 mm over the 2002-2023 period. Here, the increase due to ice-based contri-
 183 butions (+29 mm) is compensated by $>50\%$ due to continental hydrology contributions
 184 (-17 mm) (Figure 1d). The significant negative ocean mass signal here is driven by con-
 185 tributions from Asia (dark blue line in Figure 1h), including a ~ 2 mm reduction of di-
 186 rect attraction by 2023 because of water loss in the Caspian Sea. Changes in TWS in
 187 Europe have virtually no impact on sea level in the Persian Gulf (purple line in Figure
 188 1h).

189 Continental hydrology trends are ~ 0.5 mm/yr throughout the Pacific island na-
 190 tions and ice-based contributions typically contribute 70-80% of the overall ocean mass
 191 increase. During the study period, Kiribati, located in the southwest Pacific Ocean, has
 192 experienced a total ocean mass increase of 48 mm, of which 10 mm are contributed by
 193 non-ice hydrological processes (Figure 1e). Kiribati has experienced a higher proportion
 194 of ocean mass increase driven by ice mass loss compared to most other Pacific Island na-
 195 tions.

196 4.3 The 2019-2023 triple La Niña

197 During the GRACE/GRACE-FO period the El Niño Southern Oscillation (ENSO)
 198 index was mostly in its strong negative phase (>-0.5) from from mid-2010 to early 2012
 199 and again from late 2020 through to early 2023, resulting in the 2010/2011 strong La
 200 Niña and three consecutive years of La Niña conditions from 2020-2023 (Figure 2). La
 201 Niña brings significantly increased rainfall to large portions of Northern South Amer-
 202 ica and the Australian landmass (Holgate et al., 2022). These two extended periods of
 203 La Niña conditions resulted in record flooding across the eastern seaboard of Australia
 204 (Fryirs et al., 2023).

205 The earlier La Niña event of 2010/2011 caused a drop in global sea level of several
 206 millimetres as ENSO conditions transitioned from a strong El Niño event to a strong La
 207 Niña event during 2010 (Boening et al., 2012). The associated decrease in ocean mass
 208 during 2010 is visible in the GRACE record and altimetric measurements of sea surface
 209 height corrected for steric expansion of the ocean (Figure 2e). During the two-year pe-
 210 riod, ocean height reductions of -0.9 mm/yr and -0.82 mm/yr were caused by increased
 211 TWS in northern South America and Australia, respectively (Figure 2a,b). In contrast,
 212 2020-2023 saw sustained but comparatively weak La Niña conditions which caused a re-
 213 duction in the rate of ocean mass increase over the three-year period. The recent triple
 214 La Niña resulted in a more modest contribution from Australia and northern South Amer-
 215 ica to ocean mass of 0.25 mm/yr and 0.76 mm/yr, respectively. The total ocean mass
 216 measured by GRACE-FO exhibits a reduced rate of increase over this three-year period
 217 (Figure 2e). ENSO transitioned from a strong El Niño to neutral to weak La Niña con-
 218 ditions during the GRACE and GRACE-FO mission gap, this period corresponds to a
 219 2-year interruption in the increase in ocean mass measured by steric-corrected altime-
 220 try (Figure 2e).

221 The consecutive La Niña events of 2010-2012 and 2020-2023 removed a total ~ 3.44
 222 mm and ~ 3.1 mm of water from the oceans, and deposited it onto the Australian and
 223 northern South American landmasses over the two-year and three-year periods, respec-
 224 tively. These rates of TWS gain are comparable to the longer-term contributions of the
 225 polar ice sheets to the global ocean ($+0.33$ mm/yr for Antarctica, $+0.77$ mm/yr for Green-
 226 land) (Rodell et al., 2019)

227 Similar spatial patterns of change in ocean mass occurred during the two periods
 228 of consecutive La Niña events that occurred during GRACE and GRACE-FO mission
 229 operation (Figure 2c,d). However, the triple La Niña ocean increase is more localised off
 230 eastern Australia and the negative ocean mass signals in the far-field oceans are approx-
 231 imately double the magnitude in the earlier event. The increase in ocean mass around

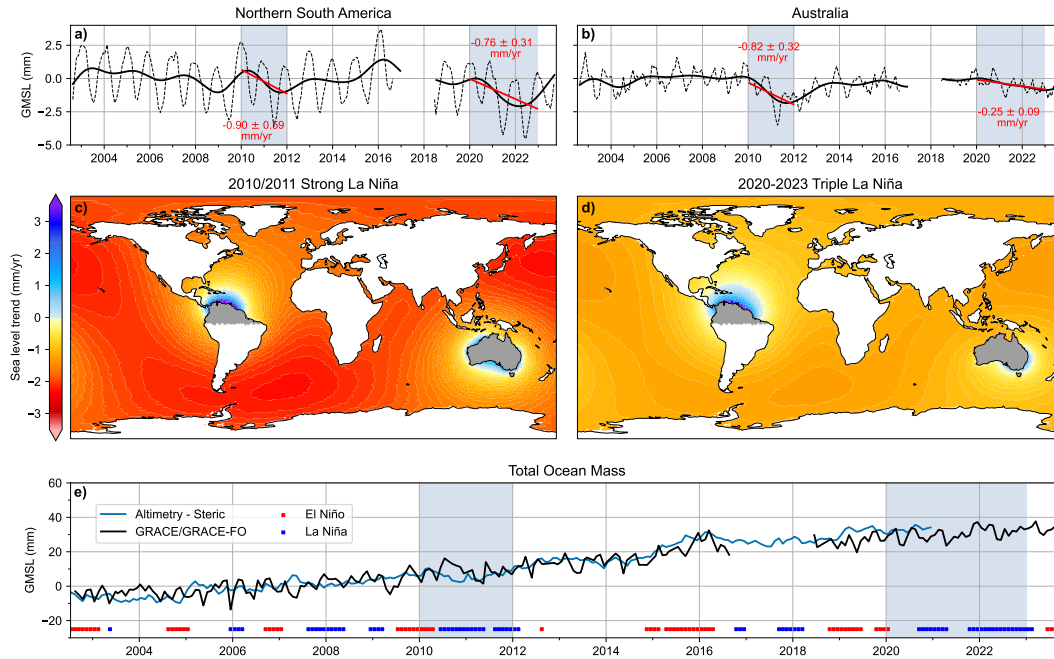


Figure 2. Change in terrestrial water storage integrated over a) northern South America, and b) the Australian continent in terms of global mean sea level (GMSL). Rate of ocean mass change derived using sea level fingerprints to apportion over the oceans the rate of change of TWS for each Australian mascon over c) the 2010-2011 La Niña event, and d) the triple La Niña period (2020-2023). GMSL from total ocean mass change measured by GRACE and GRACE-FO (black) and barystatic sea level changes from steric-corrected (blue)(Barnoud et al., 2023). The red and blue bars indicate the occurrence of El Niño and La Niña events, respectively (?, ?)

232 the coastline of Australia and northern South America during La Niña periods is due
 233 to the stronger direct gravitational attraction of the ocean to the increased water mass
 234 on each continent (Figure 2c,d). The southern Atlantic and northern Pacific Oceans lost
 235 water during the La Niña precipitation events in Australia.

236 4.4 Anthropogenic impacts on sea level

237 The combination of sea-level fingerprints and estimates of TWS changes allows the
 238 direct attribution of sea-level changes to natural climate variability and anthropogenic
 239 impacts on water storage contributions. The growing demand for water resources due
 240 to socioeconomic development and population growth has resulted in the depletion of
 241 groundwater resources in areas such as northern India and the North China Plain. Ground-
 242 water extraction in northern India (Rodell et al., 2009, 2019) is ongoing at a rate of 18
 243 Gt/yr (equivalent to +0.05 mm/yr global sea level) during the past two decades (Fig-
 244 ure 3a), causing a 1 mm increase in global sea level from 2002 to 2023. However, the rate
 245 of TWS decline in northern India during the GRACE-FO era is significantly slower at
 246 +0.02 mm/yr global sea level. Annual precipitation has not increased significantly dur-
 247 ing this time, suggesting that rates of groundwater abstraction have slowed since 2018
 248 (Figure 3a).

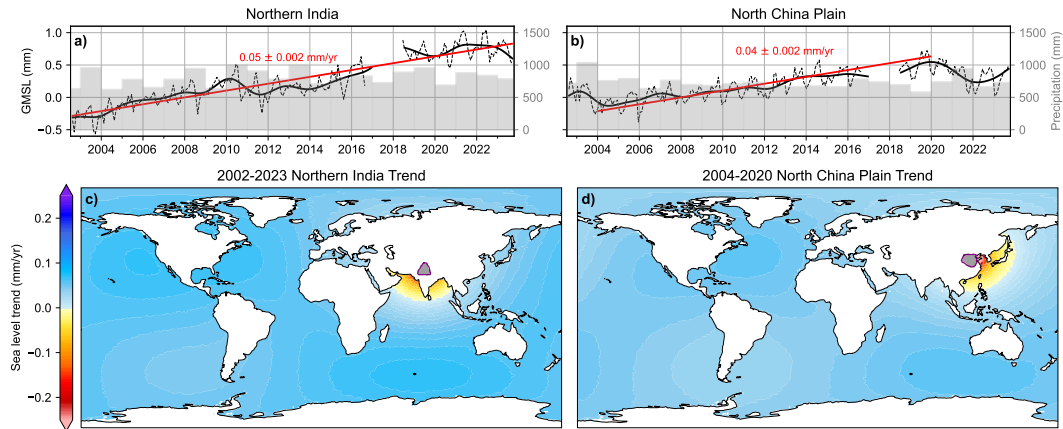


Figure 3. Time series of changes in TWS (black dashed line), low-pass filtered TWS (black solid line) and 2002-2023 and 2004-2020 TWS trends for a) northern India, and b) North China Plain, respectively, in mm of Global Mean Sea Level (GMSL). Corresponding rates of ocean mass change derived using sea level fingerprints to apportion each of these anthropogenic signals over the oceans (c,d). Mascons used to compute the ocean signals from continental hydrology in specific regions are indicated (grey). Grey bars indicate total annual precipitation in mm calculated from ERA5 monthly reanalysis (?, ?).

249 Following a record year of precipitation in 2003, TWS in the North China Plain
 250 declines, contributing $+0.04$ mm/yr to global mean sea level until 2020 (Figure 3b). The
 251 contribution of North China Plain TWS to global sea level reverses during the GRACE-
 252 FO era, storing 0.05 mm/yr of global mean sea level on the continent. This reversal in
 253 trend is likely due to the combined effect of significant increases in precipitation in 2021
 254 (Figure 3b) and decreased groundwater abstraction due to the implementation of poli-
 255 cies to reduce irrigation and south to north water diversion, resulting in groundwater recharge
 256 over GRACE-FO period (Long et al., 2020; Zhang et al., 2022). Furthermore, the increase
 257 in TWS corresponds to a reduction in water use due to the slowdown in manufacturing
 258 during the Covid-19 pandemic (Shu et al., 2023) and recharge due to environmental flow
 259 releases since 2019 (Liu et al., 2023).

260 Groundwater extraction in northern India over the GRACE and GRACE-FO pe-
 261 riod have resulted in a fall in sea level, due to a reduction in the strength of the direct
 262 gravitational attraction of the ocean to continental water stores, of a maximum nega-
 263 tive rate of -0.15 mm/yr along the coastline of southern Pakistan (Figure 3c). Ground-
 264 water extraction in the North China Plain (Rodell et al., 2019) between 2004 and 2020
 265 caused the sea level to fall in the East China Sea by up to -0.54 mm/yr during this pe-
 266 riod due to the reduced gravitational attraction of the oceans to the China landmass (Fig-
 267 ure 3d). This is almost a factor of ~ 4 greater than the signal caused by groundwater ex-
 268 traction in India because the source is much closer to the ocean, despite a comparable
 269 contribution to global mean sea level. The peak increases in ocean mass due to the ground-
 270 water extraction in India (2002-2023) and China (2004-2020) occurred in the northwest-
 271 ern Atlantic and Southern Ocean, having the largest impact on sea level in North Amer-
 272 ica and along the South Australian and South African Coastlines (Figure 3d).

273 5 Conclusion

274 Continental hydrological processes in regions that are not ice-covered have contributed
 275 to ocean mass increase on multi-decadal time-scales throughout the GRACE/GRACE-
 276 FO era. Although they contribute tens of millimetres to regional sea level in some in-
 277 stances, these impacts are not likely to persist indefinitely. For example, the Asian con-
 278 tinent, which contributed to the increase in global ocean mass (2003-2020), has been draw-
 279 ing water from the oceans since 2020. Natural climate variability, such as La Niña events,
 280 affect sea level with rates comparable to present day contributions of the polar ice sheets,
 281 although these former effects tend to persist for only a few years. Anthropogenic inter-
 282 vention, such as extraction of groundwater resources, increases ocean mass in the far field,
 283 but causes decreases in local sea level of up to ~ 1 mm/yr. These rates of near-field sea
 284 level fall are also comparable in magnitude to the longer-term contributions of the po-
 285 lar ice sheets and mountain glaciers, at times masking $\sim 80\%$ of the sea level increase caused
 286 by melting of ice-covered regions. If this extraction of groundwater ceases, then near-
 287 field regions (such as the Persian Gulf, eastern Mediterranean, East China Sea, and coast-
 288 line of southern Pakistan) would see an increase in the rate of local sea level rise of up
 289 to 1 mm/yr, significantly increasing the vulnerability of these regions to sea level rise.
 290 However, if current trends in groundwater abstraction remain, continental hydrology would
 291 continue to compound sea level rise caused by melting of continental ice in the far-field.
 292 Currently, $>25\%$ of total sea level rise around Africa, across the central Atlantic Ocean,
 293 around Australia and surrounding Pacific Island nations, and in the North Pacific Ocean
 294 are due to the declining trend in Asia's terrestrial water storage between 2002 and 2023.

295 6 Open Research

296 The GRACE and GRACE Follow-On data are available from `podaac.jpl.nasa`
 297 `.gov/dataset`. The ANU mascon solution used in this analysis (ANU_mascons_RL02)
 298 is available in netcdf format at [https://datacommons.anu.edu.au/DataCommons/rest/](https://datacommons.anu.edu.au/DataCommons/rest/display/anudc:6133)
 299 [display/anudc:6133](https://portal.auscope.org.au/) and can be visualised at <https://portal.auscope.org.au/>. The
 300 sea level fingerprints computed for our mascons are available at [add reference upon ac-
 301 ceptance of manuscript]. Barystatic sea level changes were accessed at [https://doi.org/](https://doi.org/10.24400/527896/a01-2023.012)
 302 [10.24400/527896/a01-2023.012](https://doi.org/10.24400/527896/a01-2023.012). Nino3.4 anomalies were accessed at [https://psl.noaa](https://psl.noaa.gov/gcos_wgsp/Timeseries/Nino34/)
 303 [.gov/gcos_wgsp/Timeseries/Nino34/](https://psl.noaa.gov/gcos_wgsp/Timeseries/Nino34/). ERA5 monthly averaged reanalysis total pre-
 304 cipitation was accessed at [https://cds.climate.copernicus.eu/cdsapp#!/dataset/](https://cds.climate.copernicus.eu/cdsapp#!/dataset/reanalysis-era5-single-levels-monthly-means)
 305 [reanalysis-era5-single-levels-monthly-means](https://cds.climate.copernicus.eu/cdsapp#!/dataset/reanalysis-era5-single-levels-monthly-means).

306 Acknowledgments

307 The analysis of the GRACE Follow-On data was funded in part through contracts with
 308 Geoscience Australia. R. McGirr was funded by the Australian Research Council Spe-
 309 cial Research Initiative, Australian Centre for Excellence in Antarctic Science (Project
 310 Number SR200100008).

311 References

- 312 Allgeyer, S., Tregoning, P., McQueen, H., McClusky, S., Potter, E.-K., Pfeffer, J.,
 313 ... Montillet, J.-P. (2022). ANU GRACE data analysis: Orbit modeling,
 314 regularization and inter-satellite range acceleration observations. *Jour-*
 315 *nal of Geophysical Research: Solid Earth*, 127(2), e2021JB022489. doi:
 316 <https://doi.org/10.1029/2021JB022489>
 317 Barnoud, A., Pfeffer, J., Cazenave, A., Fraudeau, R., Rousseau, V., & Ablain, M.
 318 (2023). Revisiting the global mean ocean mass budget over 2005–2020. *Ocean*
 319 *Science*, 19(2), 321–334.
 320 Boening, C., Willis, J. K., Landerer, F. W., Nerem, R. S., & Fasullo, J. (2012).

- 321 The 2011 La Niña: So strong, the oceans fell. *Geophysical Research Letters*,
 322 39(19).
- 323 Boyer, T., Domingues, C., Good, S., Johnson, G., Lyman, J., Ishii, M., . . . Wijffels,
 324 S. (2016). Sensitivity of global ocean heat content estimates to mapping meth-
 325 ods, xbt bias corrections, and baseline climatology. *Journal of Climate*, 29.
 326 doi: <https://doi.org/10.1175/JCLI-D-15-0801.1>
- 327 Chen, J., Wilson, C., Blankenship, D., & Tapley, B. (2009). Accelerated Antarctic
 328 ice loss from satellite gravity measurements. *Nature Geoscience*, 2(12), 859–
 329 862. doi: <https://doi.org/10.1038/ngeo694>
- 330 Ciraci, E., Velicogna, I., & Swenson, S. (2019). Continuity of the mass loss of the
 331 world’s glaciers and ice caps from the GRACE and GRACE follow-on missions.
 332 *Geophys. Res. Lett.* doi: <https://doi.org/10.1029/2019GL086926>
- 333 Dziewonski, A., & Anderson, D. (1981). Preliminary reference earth model. *Phys.*
 334 *Earth. Planet. Int.*, 25(4). doi: [https://doi.org/10.1016/0031-9201\(81\)90046-7](https://doi.org/10.1016/0031-9201(81)90046-7)
- 335 Fryirs, K., Zhang, N., Ralph, T. J., & Arash, A. M. (2023). Natural flood man-
 336 agement: Lessons and opportunities from the catastrophic 2023-2022 floods in
 337 eastern australia. *Earth Surface Processes and Landforms*, 48(9), 1649-1664.
 338 doi: <https://doi.org/10.1002/esp.5647>
- 339 Harvey, N., McCullough, C., & Save, H. (2022). Modeling grace-fo accelerometer
 340 data for the version 04 release. *Advances in Space Research*, 69(3), 1393-1407.
- 341 Holgate, C., Evans, J. P., Taschetto, A. S., Gupta, S., & Santoso, A. (2022). The
 342 impact of interacting climate modes on east australian precipitation mois-
 343 ture sources. *Journal of Climate*, 3147-3159. doi: <https://doi.org/10.1175/JCLI-D-21-0750.1>
- 344 Jeon, T., Seo, K.-W., Kim, B.-H., Kim, J.-S., Chen, J., & Wilson, C. R. (2021). Sea
 345 level fingerprints and regional sea level change. *earth and Planetary Science*
 346 *Letters*, 567(116985). doi: <https://doi.org/10.1016/j.epsl.2021.116985>
- 347 Kim, J.-S., Seo, K.-W., Jeon, T., Chen, J., & Wilson, C. R. (2019). Missing hy-
 348 drological contribution to sea level rise. *Geophys. Res. Lett.* doi: 10.1029/
 349 2019GL085470
- 350 Lambeck, K., A., P., & Zhao, S. (2017). The north american late wisconsin ice sheet
 351 and mantle viscosity from rebound analyses. *Quat. Sci. Rev.*, 158, 172-210.
- 352 Leblanc, M. J., Tregoning, P., Ramillien, G., Tweed, S. O., & Fakes, A. (2009).
 353 Basin-scale, integrated observations of the early 21st century multiyear
 354 drought in southeast Australia. *Water Resources Research*, 45(4).
- 355 Liu, S., Zhou, Y., McClain, M. E., & Wang, X. (2023). Effects of downstream en-
 356 vironmental flow release on enhancing the groundwater recharge and restoring
 357 the groundwater/surface-water connectivity in Yongding River, Beijing, China.
 358 *Hydrogeology Journal*. doi: <https://doi.org/10.1007/s10040-023-02675-w>
- 359 Long, D., Yang, W., Scanlon, B. R., Zhao, J., Liu, D., Burek, P., . . . Wada, Y.
 360 (2020). South-to-North Water Diversion stabilizing Beijing’s groundwater
 361 levels. *Nature Communications*, 11(1), 3665.
- 362 Loomis, B. D., Rachlin, K. E., Wiese, D. N., Landerer, F. W., & Luthcke, S. B.
 363 (2020). Replacing GRACE/GRACE-FO C₃₀ with satellite laser ranging: Im-
 364 pacts on Antarctic ice sheet mass change. *Geophysical Research Letters*, 47(3),
 365 e2019GL085488. doi: <https://doi.org/10.1029/2019GL085488>
- 366 McGirr, R., Tregoning, P., Allgeyer, S., McQueen, H., & Purcell, A. (2022). Mit-
 367 igation of thermal noise in GRACE accelerometer observations. *Advances in*
 368 *Space Research*, 69(1), 386-401.
- 369 Mitrovica, J., Gomez, N., Morrow, E., Hay, C., Latychev, K., & Tamisiea, M.
 370 (2011). On the robustness of predictions of sea level fingerprints. *Geophys.*
 371 *Res. Int.*, 187(2), 729-742.
- 372 Mitrovica, J., Tamisiea, M., Davis, J., & Milne, G. (2001). Polar ice mass variations
 373 and the geometry of global sea level change. *Rev. Geophys.*, 409, 1026-1029.
- 374 Mueller, P., & Sjogren, W. L. (1968). Mascons: Lunar mass concentrations. *Science*,

- 376 161. doi: <https://doi.org/10.1126/science.161.3842.680>
- 377 Rodell, M., Famiglietti, J. S., Wiese, D. N., Reager, J. T., Beaudoin, H. K., Lan-
378 derer, F. W., & Lo, M.-H. (2019). Emerging trends in global freshwater
379 availability. *Nature*, *557*. doi: <https://doi.org/10.1038/s41586-018-0123-1>
- 380 Rodell, M., Velicogna, I., & Famiglietti, J. S. (2009). Satellite-based estimates of
381 groundwater depletion in India. *Nature*, *460*(7258), 999–1002.
- 382 Roemmich, D., Johnson, G., Riser, S., Davis, R., Gilson, J., Brechner Owens,
383 W., ... Ignaszewski, M. (2009). The argo program: Observing the global
384 ocean with profiling floats. *Oceanography*, *22*. doi: [https://doi.org/10.5670/](https://doi.org/10.5670/oceanog.2009.36)
385 [oceanog.2009.36](https://doi.org/10.5670/oceanog.2009.36)
- 386 Rowlands, D., Luthcke, S., Klosko, S., Lemoine, F. G., Chinn, D., McCarthy, J., ...
387 Anderson, O. (2005). Resolving mass flux at high spatial and temporal resolu-
388 tion using GRACE intersatellite measurements. *Geophysical Research Letters*,
389 *32*(4). doi: <https://doi.org/10.1029/2004GL021908>
- 390 Shu, F., Lui, H., Fu, G., Sun, S., Li, Y., Ding, W., ... Zhang, L. (2023). Unraveling
391 the impact of covid-19 pandemic dynamics on commercial water-use varia-
392 tion. *Journal of Water Resources Planning and Management*, *149*(8). doi:
393 <https://doi.org/10.1061/JWRMD5.WRENG-5940>
- 394 Sun, J., Wang, L., Peng, Z., Fu, Z., & Chen, C. (2022). The sea level finger-
395 prints of global terrestrial water storage changes detected by grace and
396 grace-fo data. *Pure and Applied Geophysics*. doi: [https://doi.org/10.1007/](https://doi.org/10.1007/s00024-022-03123-8)
397 [s00024-022-03123-8](https://doi.org/10.1007/s00024-022-03123-8)
- 398 Sun, Y., Riva, R., & Ditmar, P. (2016). Optimizing estimates of annual vari-
399 ations and trends in geocenter motion and j_2 from a combination of grace
400 data and geophysical models. *Journal of Geophysical Research*. doi:
401 <https://doi.org/10.1002/2016JB013073>
- 402 Tamisiea, M. E., Hill, E. M., Ponte, R. M., Davis, J. L., Velicogna, I., & Vino-
403 gradova, N. T. (2010). Impact of self-attraction and loading on the an-
404 nual sea level cycle. *Journal of Geophysical Research*, *115*(C07004). doi:
405 <https://doi.org/10.1029/2009JC005687>
- 406 Tapley, B. D., Bettadpur, S., Watkins, M., & Reigber, C. (2004). The gravity re-
407 covery and climate experiment: Mission overview and early results. *Geophysi-
408 cal Research Letters*, *31*(9). doi: <https://doi.org/10.1029/2004GL019920>
- 409 Tapley, B. D., Watkins, M. M., Flechtner, F., Reigber, C., Bettadpur, S., Rodell,
410 M., ... others (2019). Contributions of GRACE to understanding climate
411 change. *Nature climate change*, *9*(5), 358–369. doi: [https://doi.org/10.1038/](https://doi.org/10.1038/s41558-019-0456-2)
412 [s41558-019-0456-2](https://doi.org/10.1038/s41558-019-0456-2)
- 413 Tregoning, P., McGirr, R., Pfeffer, J., Purcell, A., McQueen, H., Allgeyer, S., & Mc-
414 Clusky, S. (2022). ANU GRACE data analysis: Characteristics and benefits
415 of using irregularly shaped mascons. *Journal of Geophysical Research: Solid
416 Earth*, *127*(2), e2021JB022412. doi: <https://doi.org/10.1029/2021JB022412>
- 417 Velicogna, I., & Wahr, J. (2006). Measurements of time-variable gravity show mass
418 loss in Antarctica. *Science*, *311*(5768), 1754–1756. doi: [https://doi.org/10.](https://doi.org/10.1126/science.1123785)
419 [.1126/science.1123785](https://doi.org/10.1126/science.1123785)
- 420 Velicogna, I., & Wahr, J. (2013). ime-variable gravity observations of ice sheet mass
421 balance: Precision and limitations of the GRACE satellite data. *Geophys. Res.
422 Lett.*, *40*, 3055–3063.
- 423 Watkins, M. M., Wiese, D. N., Yuan, D.-N., Boening, C., & Landerer, F. W. (2015).
424 Improved methods for observing Earth’s time variable mass distribution with
425 GRACE using spherical cap mascons. *Journal of Geophysical Research: Solid
426 Earth*, *120*(4), 2648–2671. doi: <https://doi.org/10.1002/2014JB011547>
- 427 Wiese, D. N., Landerer, F. W., & Watkins, M. M. (2016). Quantifying and reducing
428 leakage errors in the JPL RL05M GRACE mascon solution. *Water Resources
429 Research*, *52*(9), 7490–7502. doi: <https://doi.org/10.1002/2016WR019344>
- 430 Wouters, B., S., G. A., & Moholdt, G. (2019). Global glacier mass loss during the

431 GRACE satellite mission (2002-2016). *Front. earth Sci.*, 7. doi: [https://doi](https://doi.org/10.3389/feart.2019.00096)
432 [.org/10.3389/feart.2019.00096](https://doi.org/10.3389/feart.2019.00096)
433 Zhang, Y., Zhou, W., Wang, X., Chen, S., Chen, J., & Li, S. (2022). Indian ocean
434 dipole and ENSO's mechanistic importance in modulating the ensuing-summer
435 precipitation over eastern china'. *Climate and Atmospheric Science*, 48. doi:
436 <https://doi.org/10.3389/feart.2019.00096>